Aalborg Universitet

System Architecture, Design, and Optimization of a Flexible Wireless Charger for Renewable Energy-Powered Electric Bicycles

Joseph, Peter K.; Elangovan, Devaraj; Sanjeevikumar, Padmanaban

System Architecture, Design, and Optimization of a Flexible Wireless Charger for Renewable Energy-Powered Electric Bicycles

Peter K. Joseph , *Student Member, IEEE*, Devaraj Elangovan , *Member, IEEE*,
and Padmanaban Sanjeevikumar , *Senior Member, IEEE*

Abstract—**Wireless power transmission (WPT) is one of the breakthroughs in effortless electric vehicle (EV) charging technology. Different types of wireless charger topologies were proposed and implemented to meet various constraints like power transfer efficiency, wireless transfer distance, and misalignment tolerance. Yet the coupling separation and the transfer efficiency are still underdeveloped for contactless charging of medium- and low-power EVs like e-cycles and e-scooters. For achieving the high-distance WPT in the vehicles which are prone to misalignment issues, series–series (SS) compensated WPT is used. The conventional SS-compensated WPT uses a voltage-fed converter for the power conversion. But the combination of these topologies allows reverse current flow in the system, which will affect the transfer efficiency and life span of the source. To prevent this, a reverse blocking diode or a current-fed converter can be used. Though the reverse current problem can be solved, these approaches seem to reduce the power transfer efficiency further. This article tries to optimize the current-fed converter-based SS-WPT to achieve higher coupling separation, higher power transfer efficiency, and higher misalignment tolerance than the conventional designs. To achieve this, the input inductor of the current-fed converter and the primary coil of the SS-WPT are tuned without affecting the magnetic resonance condition. The transfer efficiency was found to be 94% at a coupling separation of 200 mm, which is 20% more than the conventional voltage source inverter-based, renewable energy-powered SS-WPT charging efficiency. After proving the concept in prototype design, the results are validated by testing the same in a real-time electric cycle.**

Index Terms—**Current source inverter, electric vehicle, series–series compensator, voltage source inverter, wireless charging, wireless power transmission.**

I. INTRODUCTION

IN THE twenty-first century, energy conservation is one of the top priorities for every aspiring researcher. Modern inventions in each technological sector contribute to this purpose. If the transportation sector is considered, conventional fuel-driven vehicles are being replaced with energy-efficient electric vehicles (EVs) [1]. This combustion-free transportation holds a key role in the conservation of energy. After the invention of the EV, researchers began to concentrate on optimization of EV chargers [2]. At the beginning of the nineteenth century, the Netherlands implemented a practical prototype of battery-powered EV [3]. In 1890, William Morrison implemented a six-passenger EV in the United States, which started an EV revolution in the coming centuries [3], [4]. Even though the functional goal is the same, several topologies [5] have been introduced in the wired EV charging sector. One of the main challenges for wired charging is the individuality of charging stations by different service providers [6]. EV by a particular manufacturer cannot be charged from the charging station of another manufacturer in most of the cases [7]. For the battery charging of EVs by multiple manufactures, Zhang *et al.* [8] has introduced a multipulse based flexible rectifier for the secondary side. A single charging station for charging multiple EVs is another breakthrough in charging sector [9]. Power management scheme for such a multi-EV charging station is explained in [10].

Amidst of all these developments in conventional wired charging technology, it faces some major disadvantages. Conventional EV charging technology is based on wired transmission. Wired networks form the basis of most of the energy transmission and distribution sector. However, during the energy transmission, major energy loss occurs at transmission wires itself. The resistance R of the wire contributes to the (I^2R) loss [11]. So to reduce the transmission loss, either reduce R (by using low resistance conductor or by increasing the diameter of the conductor) and/or reduce current, I (high-voltage transmission). Both of these solutions are expensive [12]. Apart from these reasons, during wired charging, the chances of short-circuit and open-circuit are extremely likely [13]. Apart from these disadvantages, the plug point of a manufacturer needs not to be suitable for every charging points [14]. Because of these reasons, researchers began a quest for wireless charging of EVs. A plethora of systems and topologies were introduced in wireless charged EVs [15]. The invention of strongly coupled magnetic resonance (SCMR) to efficiently transmit power for more distance using magnetic resonance principle changed the wireless power transmission (WPT) direction in 2007 [16].

As always, the ultimate objective of researchers in wireless charging is to achieve more efficient power transfer for a longer

distance and the incorporation of renewable energy. To improve the power transfer efficiency and coupling separation, two areas in the wireless charger needs to be optimized—the power converter and the wireless transformer. The power converter at the input stage will invert the dc input to a high-frequency ac to ensure high quality factor of the transmitter and receiver coil and thereby increasing the power transmission capacity. The power converter at the secondary side will rectify the high-frequency ac power coming from the receiver coil to a regulated dc output to charge the battery. To increase the power transfer capacity, full-bridge converter topology is used for this purposes conventionally. The coupling separation and transfer efficiency of the wireless charger exclusively depends on the wireless transformer design. Wireless transformer basically is a combination of capacitor and inductive coil at the transmitter and receiver side to establish magnetic resonance. For this purpose, several topologies were introduced time to time mainly series–series (SS), series–parallel (SP), parallel–series (PS), and parallel–parallel (PP) [17]–[21], named after their configuration. Some advanced topologies like LCL [22] and LCC [23] topologies were derived from these fundamental designs for enhanced efficiency and performance.

Even though several topologies were proposed in the wireless charging of EVs, the charging technology for the low-/medium-power EVs is still underdeveloped. For low-power EVs like e-cycles and e-scooters, the coupling separation and power transfer efficiency are less compared to high-power EVs. An e-cycle with an electric double-layer capacitor (EDLC) as the source and WPT technology is proposed in [24]. Due to the relatively low power level of the e-cycle, the coupling separation is very less in EDLC-based wireless charging. Apart from the poor performance, the wireless charging of two-wheeler EVs faced the disadvantage of electromagnetic radiation, which should be perfectly shielded for ensuring safety [25]. Therefore, a suitable topology needs to be selected and modified for optimum performance of the low-power EV wireless charging.

For the basic WPT topology SS, the coupling separation is higher compared to other topologies; but the transfer efficiency is very low for higher distance [26]–[28]. The researchers show that SS-WPT gives better performance with voltage source inverter (VSI), as it does not affect the resonant condition [29] of WPT. But the integral combination of VSI and SS-WPT is allowing reverse current flow [30] in the system due to the high-frequency switching operation of the power converter. This reverse current flow can affect the power transfer efficiency of the charging system. In addition, the excess reverse current will damage the power source. In the case of renewable energy-powered wireless charger, this phenomena is deadly to the delicate source. To protect the source as well as to improve the performance, the reverse current should be mitigated. For this purpose, two approaches are followed. A reverse blocking diode can be used to prevent the current flow, or a current source inverter (CSI) can be used instead of VSI, as CSI is equipped with inherent reverse current blocking capability [29] due to the presence of input inductor. But the use of reverse blocking diodes will reduce the overall power transfer efficiency of the system, due to the voltage drop [31] across the diode. As this
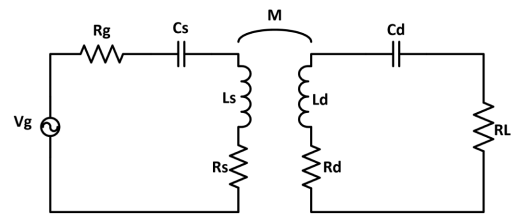

Fig. 1.   Magnetic resonance circuit.

power loss is crucial in the case of low-/medium-power EVs, the drop across the diode needs to be avoided, whereas in the case of CSI based SS-WPT, this reverse current flow is successfully mitigated. But the input inductor present in the CSI has a negative impact on the resonance condition of the wireless transformer. So whenever the input inductor is coming to the operation of SS-WPT, the coupling separation and wireless power transfer efficiency are dropping steeply [28]–[31].

The cause for the reduction in coupling separation and transfer efficiency of CSI-based SS-WPT is the distortion in magnetic resonance condition. If this challenge can be overcome, then an efficient wireless charger with high and flexible coupling separation can be designed. The factor affecting the distortion in magnetic resonance is the interaction of the input inductor of CSI and the transmitter coil. Due to this effective inductance, the transmitter side will resonate with a different frequency than that of the receiver. This phenomenon badly affects the performance of WPT. To maintain the same frequency for both transmitter and receiver, a tuning method is suggested in this article. As per the proposed technique, the value of the transmitter coil is tuned in such a way that the effective inductance in the transmitter side will generate the magnetic resonance with the same frequency. Along with the transmitter coil tuning, the entire wireless transformer is also optimized in this article. In the following sections, detailed implementation and testing of CSI-based SS-WPT is presented. The basic principles and operation of a WPT system and renewable energy-powered WPT are discussed in Section II. Section III explains the working and design of input-side inverter. The detailed hardware design and testing are discussed in Section IV.

II. Wireless Power Transmission

The basic working principle of WPT is electromagnetic induction. In order to give the wireless power a direction, a resonance concept will be used in the primary and secondary sides. It is known as strongly coupled magnetic resonance [32].

A. Basic Concept

Magnetic resonance [33] is the condition of oscillation between inductor and capacitor in the form of magnetic and electric field, respectively. The standard circuit diagram of a wireless power transfer system is shown in Fig. 1. In magnetic resonance circuit, the energy oscillation and transmission can be done with sufficient excitation. If the resonating energy in the system is more than the losses in elements, it stagnates and transfers to the secondary coil. In Fig. 1, V_g is the primary voltage and R_g is
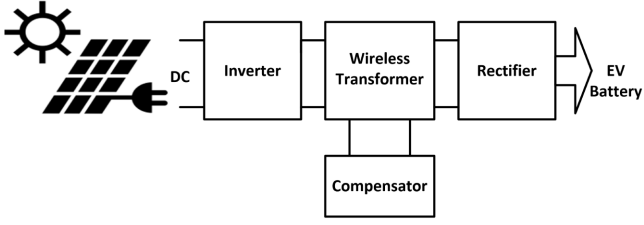
This article has been accepted for inclusion in a future issue of this journal. Content is final as presented, with the exception of pagination.

JOSEPH *et al.*: SYSTEM ARCHITECTURE, DESIGN, AND OPTIMIZATION OF A FLEXIBLE WIRELESS CHARGER

3

Fig. 2. Functional block diagram of renewable energy-driven EV.

Fig. 3. Basic compensator topologies. (a) Series-Series, (b) Series-Parallel, (c) Parallel-Series, and (d) Parallel-Parallel.

the input source resistance. C_s and C_d are the source and device capacitance, respectively. L_s and L_d are the source and device inductor coils; R_s and R_d are the source and device parasitic resistance correspondingly. With the proper excitation, it will oscillate at a resonant frequency of

$$\omega_o = \frac{1}{\sqrt{LC}}. \tag{1}$$

The transmission efficiency of a WPT system depends on its quality factor Q.

$$Q = \sqrt{\frac{L}{C}} \cdot \frac{1}{R} = \frac{\omega_o L}{R} \tag{2}$$

As quality factor is high, transfer efficiency also will be high. From (2), it is clear that, in order to maintain a high quality-factor of inductor coils of WPT, the winding resistance should be minimized. For this purpose, high standard materials like Litz wire can be used [14].

B. Renewable Energy-Powered Wireless Charging

The location of most of the parking slots is with abundance of solar energy exposure. With the proper arrangement of solar panel on the roof, it will simultaneously function as parking slot and charging station [30].

Fig. 2 shows the block diagram of renewable energy-powered EV. Here the dc input from the renewable energy-extracting system is converted to high-frequency ac with an inverter. This power is transferred from primary to secondary through a wireless transformer and ac–dc rectifier. For conventional grid-connected wireless charges, the input will be ac.

In a wireless transformer, the coupling coefficient will be very much less than 0.3, whereas it is more than 0.9 for wired transformers. Due to the loose coupling, the leakage inductance of wireless transformer will be far high. In order to balance the effects of leakage inductance, compensator networks are used. A compensator network is an arrangement of capacitors and/or inductors with respect to the primary and secondary coils. There are mainly four types of basic compensators available such as series–series (SS) [18], series–parallel (SP) [19], parallel–series (PS) [20], and parallel–parallel (PP) [21].

Fig. 3 illustrates the basic compensator topologies in WPT. In compensator design, the secondary capacitor is designed using the basic resonant frequency (1).

The primary capacitor design varied according to the type of compensator. If we observe various design equations [14], out of four fundamental compensators, only SS design does not
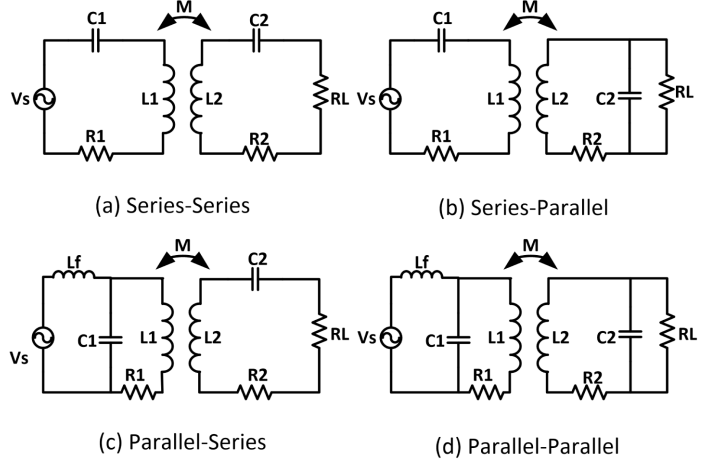
depend on the coupling coefficient. It means SS compensator maintains its resonance operation throughout the coupling separation, without affecting transfer efficiency. So for designing a flexible distance wireless charger, the SS configuration can be used.

However, while integrating the renewable energy power source with the conventional compensator topology, the reverse current flow needs to be considered. As the renewable energy source is dc in nature and the transmitter-side coil requires an ac power, a high-frequency inverter is mandatory for the wireless charger. Due to the high-frequency switching of the transmitter-side inverter, a reverse current flow will occur in the primary. This reverse current flow can damage the delicate renewable source. As reverse blocking diode causes a considerable power loss in the system, a CSI can be used for mitigating the reverse current. But the inductor interaction of CSI distorts the magnetic resonance as explained in the previous section. To prevent that, a proper inductance tuning approach needs to be followed, as discussed in the next section.

III. PRIMARY-SIDE INVERTER

Either VSI or CSI can be used for converting dc to high-frequency ac. VSI is the most commonly used inverter topology for wireless charger applications. But there is no facility for preventing reverse current flow in VSI topology. If charging station is powered by renewable energy, as mentioned earlier, the delicate charging system needs to be protected from all kind of reverse currents. If the EV battery requires a constant current supply, VSI will not be a right choice.

CSI has several advantages over VSI, including the inherent capability to block reverse current flow, reduction of current ripples, boosting ability, reduction of magnetic elements size, etc. Compared to VSI, an additional inductor is connected in series with the source. If one operating cycle is divided from T_0 to T_8, there are following six operating modes for CSI-based WPT:

1) S1, S2, S3, and S4 ON condition (from T_0 to T_1);
2) S1 and S2 ON and D3 and D4 conducting (from T_1 to T_3) ;

This article has been accepted for inclusion in a future issue of this journal. Content is final as presented, with the exception of pagination.

4   IEEE SYSTEMS JOURNAL
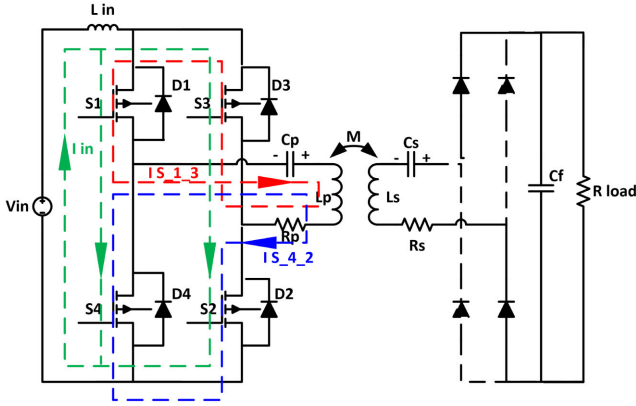
Fig. 4.   CSI—WPT mode 1 circuit diagram.
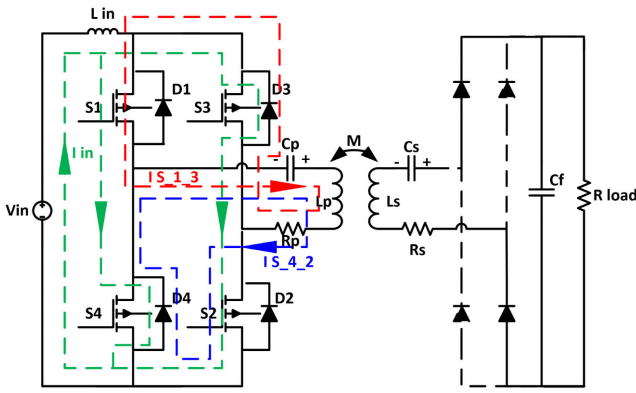

Fig. 5.   CSI—WPT mode 2 circuit diagram.

3) S1 and S2 ON (from T_3 to T_4);
4) S1, S2, S3, and S4 ON (from T_4 to T_5);
5) S3 and S4 ON and D1 and D2 conducting (from T_5 to T_7);
6) S3 and S4 ON (from T_7 to T_8).

1) Mode 1. S1, S2, S3, and S4 ON (T_0–T_1): At T_0, capacitor Cp will be in negative polarity due to current flow through S3 and S4 in the previous cycle. At T_0, S1 and S2 are turned ON and S3 and S4 are already ON.

Fig. 4 shows the circuit diagram of mode 1 operation of CSI-based WPT. As C and L are in resonance, at T_0, capacitor starts discharge from $-V_C$max toward positive. At T_0, I_{Lin} was zero. As transformer is disconnected, L_{in} starts charging. At T_1, S3 and S4 turned OFF.

$$I_{S1} = I_{S2} = \frac{1}{2}\left(I_{in} + (I_{Lp}(t))\right)$$

$$I_{S3} = I_{S4} = \frac{1}{2}\left(I_{in} - (I_{Lp}(t))\right) \quad (3)$$

2) Mode 2. S1 and S2 ON and D3 and D4 Conducting (T_1–T_3): At T_1, capacitor C_p will continue to be in negative polarity as the previous cycle.

Fig. 5 shows the circuit diagram of mode 2 operation of CSI-based WPT. At T_1, S3 and S4 are turned OFF, but D3 and D4 are forward-biased. The current flow is shown in the figure. At T_2, capacitor discharges completely and $V_{Cp} = 0$. Inductor current $I_{Lp} = I_L$max. Diode current I_{D3} and I_{D3} follows the pattern of

Fig. 6.   CSI—WPT mode 3 circuit diagram.

I_{Lp} in negative polarity.

$$I_{S1} = I_{S2} = \frac{1}{2}\left(I_{in} + (I_{Lp}(t))\right)$$

$$I_{D3} = I_{D4} = \frac{1}{2}\left(I_{in} - (I_{Lp}(t))\right) \quad (4)$$

From T_2 to T_3, capacitor charges in positive polarity with inductor discharging current I_{Lp}. At T_3, $I_{in} = I_{Lp}(t)$.

3) Mode 3. S1 and S2 ON (T_3–T_4): At T3, D3 and D4 stopped conduction. Input and discharging current of L_{in} appear across the primary.

Fig. 6 shows the circuit diagram of mode 3 operation of CSI-based WPT. At T_3, I_{Lin} is maximum and starts discharging. At T_4, the voltage across the capacitor is $+V_C$max. At T_4, inductor current I_{Lp} is zero.

$$V_{in} = (L_{in} + L_p)\frac{dI_{in}}{dt} + \frac{1}{Cp}\int I_{in}dt - M\frac{dI_{out}}{dt} + R_pI_{out}$$

$$0 = \frac{1}{Cs}\int I_{out}dt + L_s\frac{dI_{out}}{dt} - M\frac{dI_{in}}{dt} + (R_s + R_{load})I_{out}$$

$$(5)$$

4) Mode 4. S1, S2, S3 and S4 ON (T_4–T_5): At T_4, capacitor Cp will be in positive polarity due to current flow through S1 and S2 in the previous cycle. At T_4, S3 and S4 are turned ON and S1 and S2 are already ON. The current flow is shown in the figure. Fig. 7 shows the circuit diagram of mode 4 operation of CSI-based WPT. As S3 and S4 turned ON, its current starts increasing. And in S1 and S2, current starts decreasing. As C and L are in resonance, at T_4, the capacitor starts to discharge from $+V_C$max toward negative. At T_4, I_{Lin} was zero. At T_5, S1 and S2 turned OFF.

$$I_{S1} = I_{S2} = \frac{1}{2}\left(I_{in} - (I_{Lp}(t))\right)$$

$$I_{S3} = I_{S4} = \frac{1}{2}\left(I_{in} + (I_{Lp}(t))\right) \quad (6)$$

5) Mode 5. S3 and S4 ON and D1 and D2 Conducting (T_5–T_7): At T_5, capacitor Cp will continue to be in negative polarity as the previous cycle. At T_5, S1 and S2 are turned OFF, but D1 and D2 are forward-biased. The current flow is shown in the figure.

Fig. 7.   CSI—WPT mode 4 circuit diagram.

Fig. 8.   CSI—WPT mode 5 circuit diagram.

Fig. 8 shows the circuit diagram of mode 5 operation of CSI-based WPT. At T_5, S1 and S2 turned OFF. At T_6, capacitor discharges completely and $V_{Cp} = 0$. Inductor current $I_{Lp} = -I_L$max. Diode current I_{D1} and I_{D2} follows the pattern of I_{Lp} in reverse polarity.
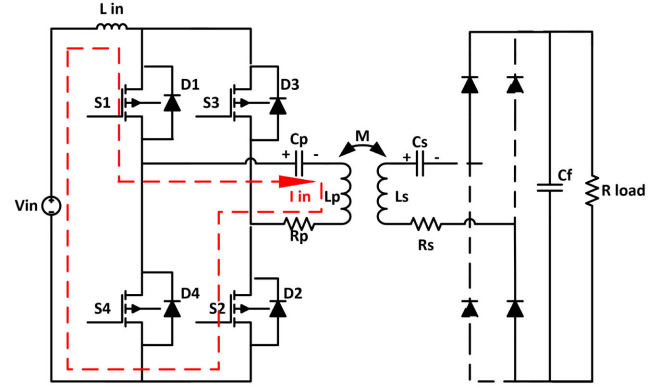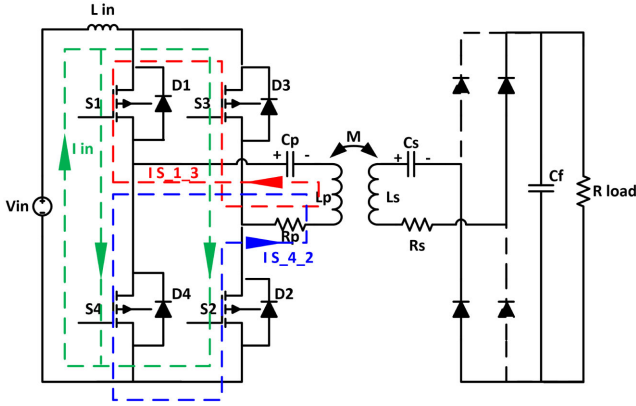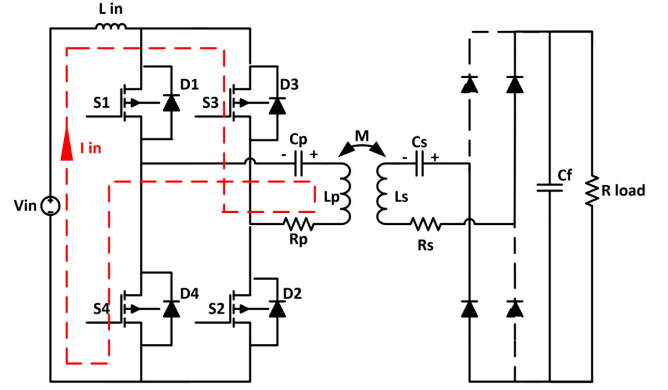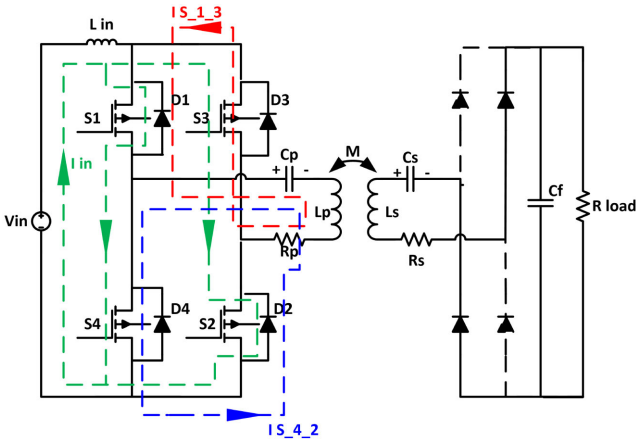
$$I_{S1} = I_{S2} = \frac{1}{2}\left(I_{\text{in}} - (I_{Lp}(t))\right)$$

$$I_{D3} = I_{D4} = \frac{1}{2}\left(I_{\text{in}} + (I_{Lp}(t))\right) \tag{7}$$

From T_6 to T_7, capacitor charges in positive polarity with inductor discharging current I_{Lp}. I_{Lin} continues charging and the source remains disconnected from secondary. At T_3, $I_{\text{in}} = I_{Lp}(t)$. As per (11), diode current becomes zero. D1 and D2 stop conduction. Now short-circuit condition is absent and the source is connected to secondary. L_{in} starts discharging. Source voltage and input inductor stored voltage are added up and fed to the primary.

6) Mode 6. S3 and S4 ON (T_7–T_8): At T_7, D1 and D2 stopped conduction. Input and discharging current of L_{in} appear across the primary. Capacitor still continues to charge in reverse direction.

Fig. 9 shows the circuit diagram of mode 6 operation of CSI-based WPT. At T_7, I_{Lin} is maximum and starts discharging. At

Fig. 9.   CSI—WPT mode 6 circuit diagram.

T_8, the voltage across the capacitor is $-V_C$max. At T_8, inductor current I_{Lp} is zero.

$$V_{\text{in}} = V_{Lin} + V_{Cp} + V_{Lp} + V_M + V_R$$

$$V_{\text{in}} = (L_{\text{in}} + L_p)\frac{dI_{\text{in}}}{dt} + \frac{1}{Cp}\int I_{\text{in}}dt - M\frac{dI_{\text{out}}}{dt} + R_p I_{\text{out}}$$

$$0 = \frac{1}{Cs}\int I_{\text{out}}dt + L_s\frac{dI_{\text{out}}}{dt} - M\frac{dI_{\text{in}}}{dt} + (R_s + R_{\text{load}})I_{\text{out}} \tag{8}$$

As the input-side inductor will store energy when the source is separated from the load and will give back that energy in the next cycle, the inductor value can be reduced compared to that of VSI configuration to achieve the same performance. Since CSI will block reverse current, no diode is required in the primary. With these two characteristics, high efficiency can be achieved. But with the integration of an inductor in the source, the resonance condition of SS compensator should not be affected.

IV. DESIGN

The topologies for compensator and inverter are selected. Now the WPT system should be designed with maximum performance.

A. CSI Inverter

The resonance frequency condition for SS-compensated WPT is given by

$$\omega_o = \frac{1}{\sqrt{L_P C_P}} = \frac{1}{\sqrt{L_S C_S}}. \tag{9}$$

The frequency ω_s of supply voltage fed to the primary should be equal to the designed resonant frequency for efficient wireless transmission. Consider an input inductor L_{in} is connected in series with the source for converting it into current fed. During the forward conduction mode, L_{in} will come in series with primary inductance L_P. Now the effective inductance of primary side in series with capacitor C_S will become $L_{\text{in}} + L_P$. So the primary-side resonant frequency becomes

$$\omega_1' = \frac{1}{\sqrt{(L_{\text{in}} + L_P)C_P}}. \tag{10}$$

As the supply frequency ω_s and secondary-side resonant frequency ω_2 remain unchanged, there will be a conflict in the frequency between primary-side supply voltage, the primary coil, and secondary coil.

$$\omega_s = \omega_o = \frac{1}{\sqrt{L_S C_S}} \neq \frac{1}{\sqrt{(L_{\text{in}} + L_P)C_P}} \quad (11)$$

This frequency conflict is the reason why current-fed designs are omitted in conventional designs. To mitigate this conflict, the primary coil should be modified in such a way that $L'_P = L_P - L_{\text{in}}$, where L'_P is the new primary inductance value. The value of L_{in} will always choose less than L_P to ensure smooth operation of WPT and minimize the winding losses. The primary-side resonant frequency will be changed to

$$\omega'_1 = \frac{1}{\sqrt{(L_{\text{in}} + L'_P)C_P}} = \frac{1}{\sqrt{(L_{\text{in}} + (L_P - L_{\text{in}}))C_P}}$$

$$= \frac{1}{\sqrt{L_P C_P}} = \omega_o. \quad (12)$$

Now the supply voltage frequency, primary coil frequency, and secondary coil frequency will be the same as in the case of conventional voltage-fed SS-WPT, hence the frequency conflict is mitigated.

B. Wireless Transformer

Every wireless transformers are designed for a particular coupling coefficient k, to get the desired output voltage in open loop. In the design, we will fix the primary inductance L_1 first, based on the current flowing and winding loss. Then, secondary inductance L_2 is determined by fixing the coupling coefficient, to get the desired output voltage using the following equations:

$$M = k\sqrt{L_1 L_2}$$

$$\frac{V_2}{V_1} = k \cdot \frac{N_2}{N_1} = k \cdot \frac{L_2}{L_1} \quad (13)$$

where V_2 and V_1 are the secondary and primary voltages, respectively; N_2 and N_1 are the secondary and primary number of turns. By knowing the value of V_2, V_1 and fixing k, L_2 can be determined using (12) and (13). Most of the papers [16]–[26] designed transformer with $0.3 < k < 0.5$ to minimize the winding losses. As "k" reduces, L will increase, so does the winding losses. But the effect of winding design has a severe impact on transmission efficiency. A higher efficiency wireless transformer model is proposed here.

A commonly adopted WPT design [16]–[28] with designed coupling factor $k = 0.33$ is analyzed here. At this designed separation, the output voltage will be the same as that of designed voltage as in (13). Here the designed output voltage is 48 V. A PSIM simulation of SS-compensated wireless power transformer designed for $k = 0.33$ is created. To check the variable distance compatibility of the selected design, the value of k is gradually reduced from $k = 0.33$ to $k = 0.02$ and tabulated the performance values as shown in Table I.

Fig. 10 illustrates the PSIM simulation of conventional VSI-based SS-WPT. The WPT parameters are obtained from [19].

TABLE I
PERFORMANCE OF THE CONVENTIONAL TRANSFORMER DESIGNED
WITH $k = 0.33$

K	Output Voltage (V)	Output Power (W)	Efficiency (%)
0.3	47.78	95.12	97.22
0.25	56.63	133.62	96.27
0.2	69.86	203.35	94.49
0.15	89.72	335.40	90.91
0.1	122.19	622.09	81.98
0.05	161.66	1088.91	53.59
0.02	119.10	591.03	15.65
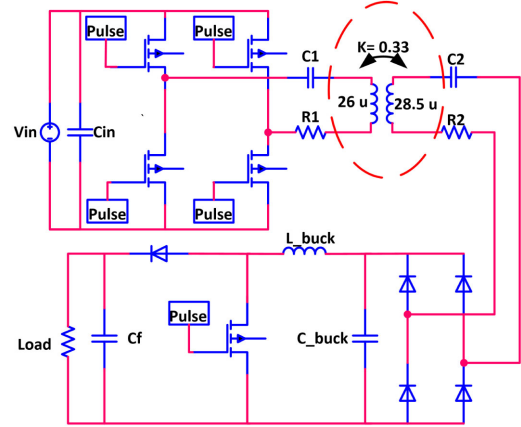
Fig. 10. PSIM simulation of conventional VSI WPT.
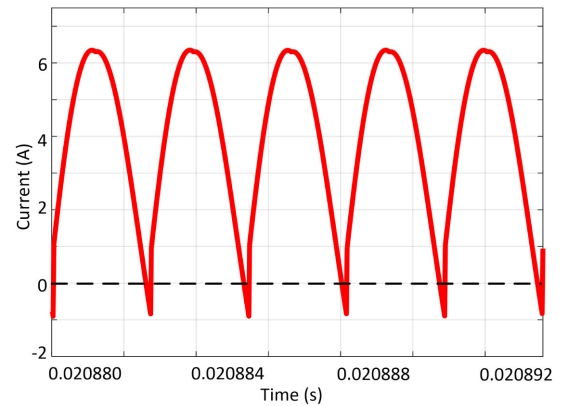
Fig. 11. PSIM simulation of conventional voltage-fed WPT.

For preventing the reverse current, no blocking diodes are used in the circuit. As there is no provisions for mitigating the reverse current flow, there will be a current flow in the direction of source. This can cause functional damage in the source. The enhanced waveform of the source current corresponding to the voltage-fed SS-WPT is illustrated in Fig. 11. A reverse current flow exists in the circuit. As the input power increases, this reverse current also will increase, which will cause major troubles. The range of reverse current will increase for higher coupling separations. This may damage the delicate power supply systems.

This article has been accepted for inclusion in a future issue of this journal. Content is final as presented, with the exception of pagination.

JOSEPH *et al.*: SYSTEM ARCHITECTURE, DESIGN, AND OPTIMIZATION OF A FLEXIBLE WIRELESS CHARGER

7

K	Output Voltage (V)	Output Power (W)	Efficiency (%)
0.3	8.45	2.97	98.54
0.25	10.12	4.27	98.51
0.2	12.62	6.64	98.47
0.15	16.77	11.71	98.09
0.1	24.97	25.97	97.43
0.05	48.09	96.36	93.84
0.02	95.53	380.01	74.6

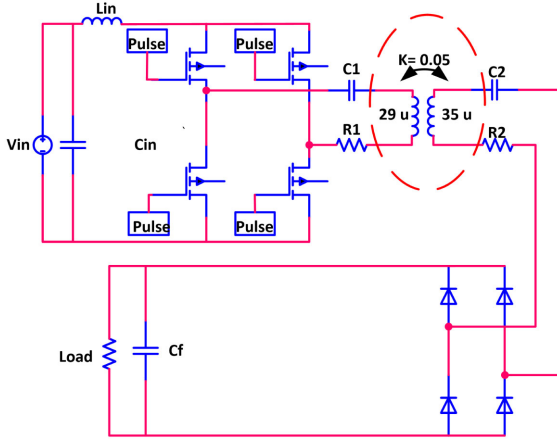Fig. 12.   PSIM simulation of modified WPT.

Fig. 13.   PSIM simulation of proposed current-fed WPT.

The variation of transfer efficiency with varying coupling for a high k transformer is shown in Table II. The coupling coefficient is varied from 0.3 to 0.02.

As the WPT is designed for an output voltage of 48 V at the selected coupling coefficient of $k = 0.33$, it is delivering the rated output at the same coupling separation.. The load resistance is considered as 24 Ω for the simulation. But the transfer efficiency of transformer drastically reduces with increased transfer distance [17]–[30], especially after $k < 0.15$.

For analyzing the effect of coupling coefficient in wireless transformer design, the designing k value is reduced to 0.05 from the 0.33 of conventional design. The simulation of the modified system is illustrated in Fig. 12. The L_{in} and new L_1 are designed using (12) for maintaining the resonance frequency same. The value of L_2 is increased from 28.5 to 36 μH to get the required output of 48 V using (13). Apart from the input inductor and coil modification, the secondary-side buck converter is removed for compact size and simple transmitter-side control.

The enhanced input current waveform of the proposed current-fed SS-WPT operating at a reduced coupling coefficient of $k = 0.05$ is illustrated in Fig. 13. For obtaining the same output voltage of 48 V as in the voltage-fed case, the reverse current is successfully mitigated in the simulation. Though the average current is the same in both cases, the peak current also reduced in the current-fed case. This reduced peak current and mitigated reverse current will effect in an improved power transfer efficiency. This indicates that the proposed CSI-based SS-WPT can successfully solve the reverse current without affecting the WPT.
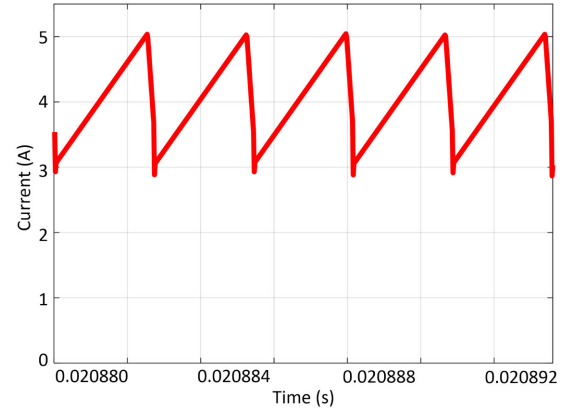
Table II shows the variation of transfer efficiency with varying coupling for a low k transformer. As it designed for an output voltage of 48 V, at the designed coupling coefficient $k = 0.05$, it delivers 48 V. If we compare the performance of conventional and proposed design at a maximum distance like $k = 0.02$, the transfer efficiency of conventional design is 15.65%, whereas that of the proposed design is 74.6%. This satisfies the higher separation tolerance requirement in [27] and [28]. This proves the effectiveness of the proposed inductance tuning approach with CSI-based SS-WPT. Even though the efficiency is improved considerably, the output voltage is drastically varying with the coupling variation. To obtain a regulated voltage at the output side, a closed-loop control needs to be designed.

C. Closed-Loop Control

From the mode equations derived in Section III, the open-loop transfer function of the proposed current-fed SS-WPT can be obtained using state-space analysis [33] as follows:

$$G(s) = \frac{6 \times 10^{-5}s + 60}{2.525 \times 10^{-9}s^2 + 2.701 \times 10^{-5}s + 1.01}. \quad (14)$$

From the open-loop transfer function, the closed-loop controller can be designed using the Bode plot method as in [34], by giving sufficient gain and phase margin with optimum pole-zero injection.

Since the switching frequency is selected as 200 kHz, the bandwidth of the proposed system is fixed as 20 kHz. Since the gain of open-loop transfer function $G(s)$ is not 0 dB at the bandwidth, a controller $H(s)$ is designed to give sufficient compensation at 20 kHz. For providing a sufficient phase margin, zeros are added to the design. The final controller transfer is obtained as

$$H(s) = \frac{5.995 \times 10^5 s^2 + 1.47 \times 10^{10}s + 9.007 \times 10^{13}}{s^3 + 7.034 \times 10^5 s^2 + 1.136 \times 10^{11}s}. \quad (15)$$

And the closed-loop transfer function will be

$$Y(s) = G(s) \times H(s). \quad (16)$$

The final Bode plot representation of $G(s)$, $H(s)$, and $Y(s)$ are illustrated in Fig. 14. With the proper controller design, the
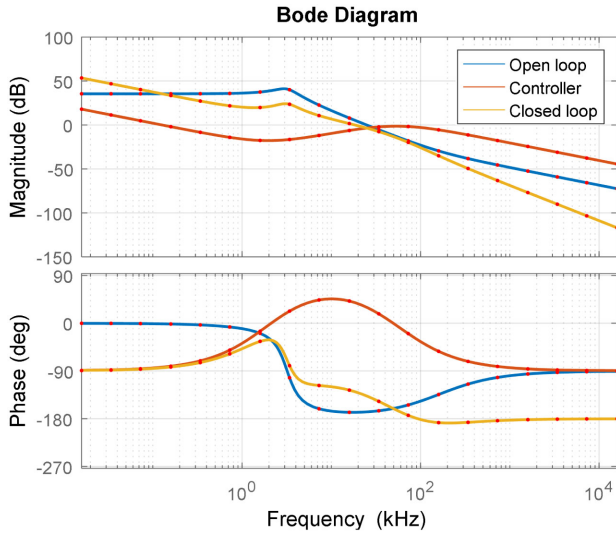
Fig. 14.   Bode plot of open-loop, controller, and closed-loop functions.
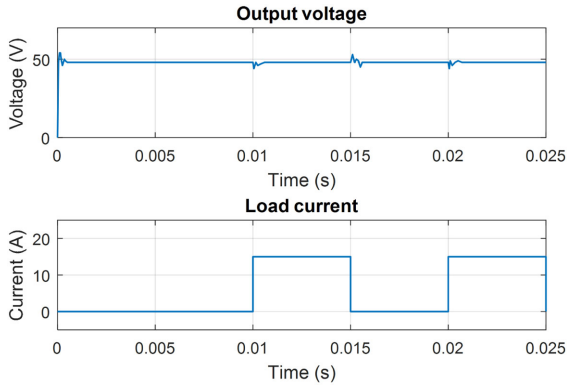

Fig. 15.   Stability testing of the controller in Matlab.

closed-loop transfer function having a perfect gain margin and phase margin is illustrated. Now the feasibility of the controller needs to be validated in simulation.

The closed-loop testing of the controller is illustrated in Fig. 15. In the closed-loop system, load dynamics are inserted after attaining the steady state. The output is returning to the steady state of 48 V in 1 ms of settling time. Therefore, the proposed CSI-based SS-WPT and its linear control are proved in simulation. Now the same has to be validated in hardware. Hence, the system is stabilized now.

V. HARDWARE IMPLEMENTATION

To validate the theoretical and simulated outcomes, the hardware is needed to be implemented. As an initial prototype, the parameters were chosen minimum. Table III tabulates the list of parameters used for prototype development. Coil design is the most delicate part of a WPT system. Winding resistance increases the I^2R loss in the transformer and affects the transmission efficiency severely. The most feasible solution to this problem is Litz wire [14], [27], [28]. By increasing the number of strands, the winding resistance can be reduced. In the proposed method, we used a 40 AWG × 800 strands Litz wire, which

TABLE III
HARDWARE DESIGN PARAMETERS

Parameter	Value
Input voltage	9 V - 27 V (Programmable DC power supply)
Output voltage	48 V
Output power	96 W
Input inductor	8 μH
Transmitter coil	29 μH, 290 mm x 290 mm
Receiver coil	35 μH, 290 mm x 290 mm
Ferrite shielding	300 mm x 300 mm x 2 mm
Switching frequency	200 KHz
Receiver capacitor	18 nF
Transmitter capacitor	20 nF
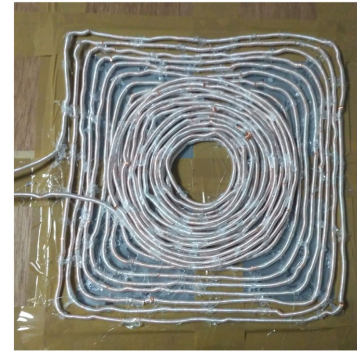
Fig. 16.   36 μH inductor.

constitutes lesser winding resistance for 36 μH, than that of 28.5 μH in [26].

Fig. 16 illustrates the fully fabricated wireless receiver (36 μH) coil. Similarly, transmitter (29 μH) coil is fabricated, both having a size of 290 mm × 290 mm. To obtain maximum mutual inductance during the wireless transmission, square shape is adapted for fabrication [35]. To shield the electronic apparatus and metallic objects from electromagnetic radiation, a ferrite sheet of 300 mm × 300 mm × 3 mm is used behind both primary and secondary coils. Transmitter coil uses a 13 number of turns of Litz wire to contribute 26 μH, whereas receiver coil uses 27 number of turns for 36 μH inductance.

The hardware test setup of the proposed design with dc electronic load is illustrated in Fig. 17. In the prototype design, the primary coil is connected with programmable dc source and current-fed inverter. The secondary coil of WPT is connected to a rectifier and dc electronic load. The switching control was done using Dspace controller at a switching frequency of 200 kHz. The input is varied from 9 to 27 V and load is varied from 0 to 70 Ω. The coupling separation is varied to analyze the effect of each parameter individually. With a minimum coupling separation of 1 mm between the coils, a minimum input voltage of 2 V with some injected noise at the programmable power supply and a moderate duty of 0.5, the testing is initiated. Voltage is slightly increased to 8 V, then the coupling separation between coils is increased gradually to a maximum of 30 cm, where efficiency began to reduce drastically. Because of the proposed transformer design, efficiency seemed to be stable and higher compared to the available renewable energy-powered WPT techniques [24], [28], where maximum efficiency was noted to be 75%.
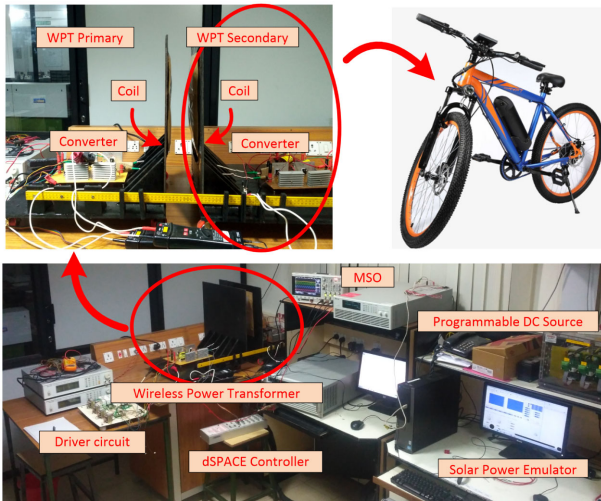
This article has been accepted for inclusion in a future issue of this journal. Content is final as presented, with the exception of pagination.

JOSEPH *et al.*: SYSTEM ARCHITECTURE, DESIGN, AND OPTIMIZATION OF A FLEXIBLE WIRELESS CHARGER 9

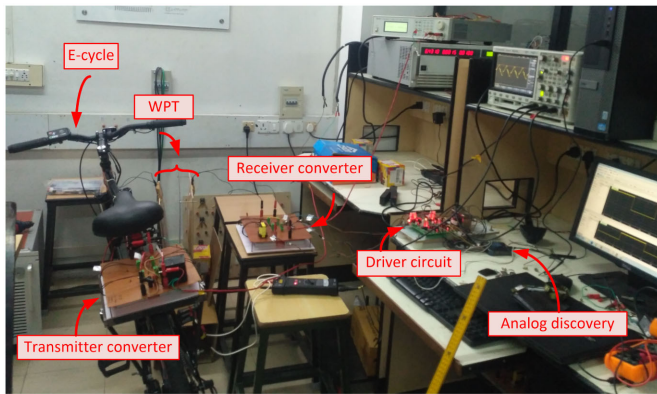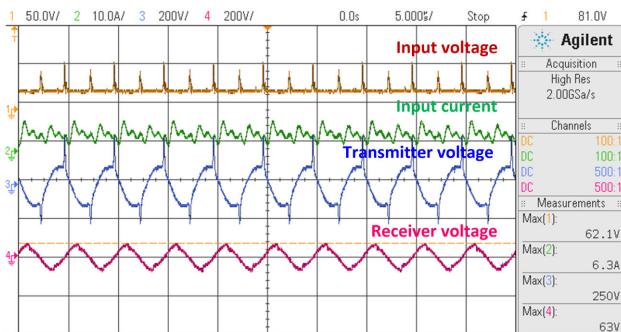Fig. 17. Hardware testing setup with dc electronic load.

Fig. 18. Wireless charging of e-cycle with proposed system.

Fig. 19. WPT waveforms at a coupling separation of 15 cm at an input voltage and load of 25 V and 24 Ω, respectively.

After proving the concept of the proposed current-wed wireless charger, the system is integrated with a real-time e-cycle and validated the results. The test setup with the actual e-cycle is illustrated in Fig. 18.

Fig. 19 illustrates the input and WPT coil waveforms at a coupling separation of 15 cm. In the hardware waveforms, the reverse current is successfully mitigated due to the current-fed inverter design. The transmitter and receiver coil voltages have a switching frequency of 200 kHz. If the input voltage, input
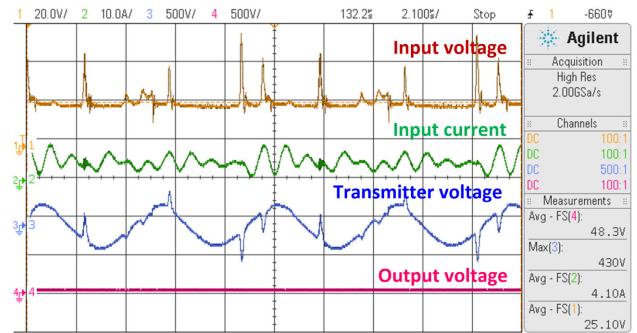
Fig. 20. Performance waveforms of the proposed WPT at a coupling separation of 20 cm at an input voltage of 25 V and load 24 Ω.
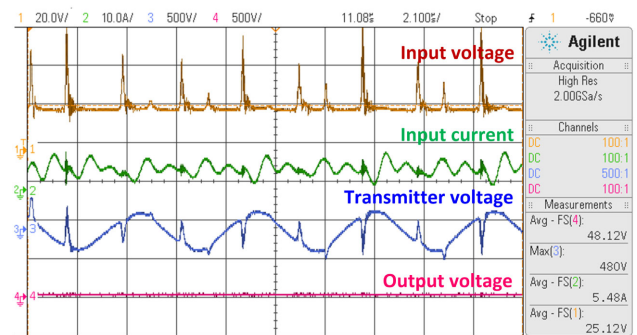
Fig. 21. Performance waveforms of the proposed WPT at a coupling separation of 30 cm at an input voltage of 25 V and load 24 Ω.

current, output voltage, and output load are known, the overall efficiency of the system can be calculated using the equation

$$\eta = \frac{V_{\text{out}}^2 / R_{\text{load}}}{V_{\text{in}} \times I_{\text{in}}}. \tag{17}$$

The performance waveforms of the proposed current-fed SS-WPT at a coupling separation of 20 cm at an input voltage of 25 V and load resistance of 24 Ω is illustrated in Fig. 20. As the parameters are known, the overall efficiency of 94.3% can be obtained using (17). The output voltage is 48.3 V. The performance waveforms of the proposed current-fed WPT at an increased coupling separation of 30 cm are shown in Fig. 21. As visible in the figure, voltage ripple is increased with the increase in coupling separation. Though the distance is increased with the same input voltage and load resistance, due to the closed loop, the output voltage remains the same at 48 V.

At this operating condition, the efficiency can be calculated as 70%. Similarly, performance waveforms are taken for various operating conditions, by varying the coupling separation from 0 to 30 cm and input voltage from 4 to 25 V. The output voltage is approximately maintained at 48 V at all the conditions. And input reverses current flow was absent throughout the operation.

Fig. 22 illustrates the detailed analysis of the relationship between efficiency and coupling separation for the variation in input voltages with given noise. If the coupling separation is analyzed, a clear efficiency peak is visible at a separation of 20 cm, where the system attains the maximum efficiency condition [14]. Maximum efficiency of 94% is obtained at a higher separation of 20 cm, input voltage of 25 V, an output load
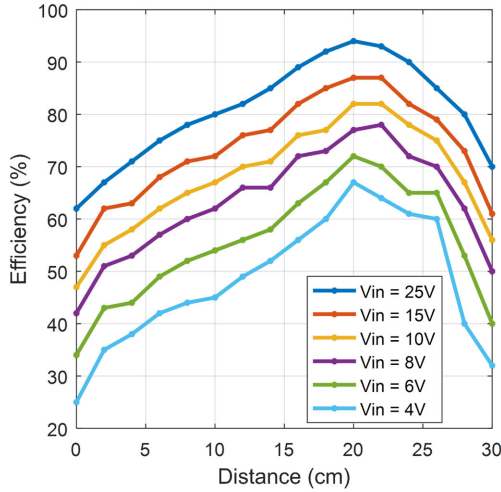
Fig. 22.   Efficiency vs. coupling separation plot for different input voltages.
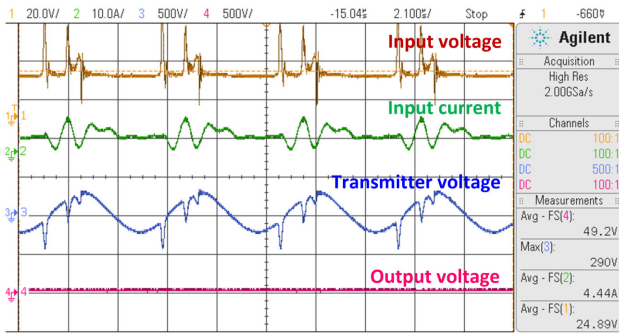

Fig. 23.   Performance waveforms of the proposed WPT with an increased load of 30 Ω at 25 V input and 20 cm separation.

of 10 Ω, and a duty of 0.5. If the known values are substituted in the maximum efficiency condition [14]

$$k = \sqrt{\frac{Z_o^2 - R^2}{(2\pi f)^2 L_1 L_2}}. \qquad (18)$$

From (18), $k = 0.259$, which corresponds to maximum efficiency separation of 20 cm in the designed WPT system. The variation of load, duty, and input voltage have a major impact on defining efficiency. The load is varied up to 70 Ω to study the effect.

Fig. 23 shows the input and output performance waveform of implemented current-fed SS-WPT system at a higher load of 30 Ω at a coupling separation of 20 cm. Even though the supplied input voltage contains considerable noises, the proposed system is able to provide a regulated output of 48 V across the terminals with the closed-loop operation. Here also, the power transfer efficiency can be found out using (17). The overall efficiency of the system for 30 Ω load is obtained as 85.12%, which is far better compared to the conventional systems which are operating under lower load conditions. As the load decreases, efficiency will increase, but the load voltage remains the same.
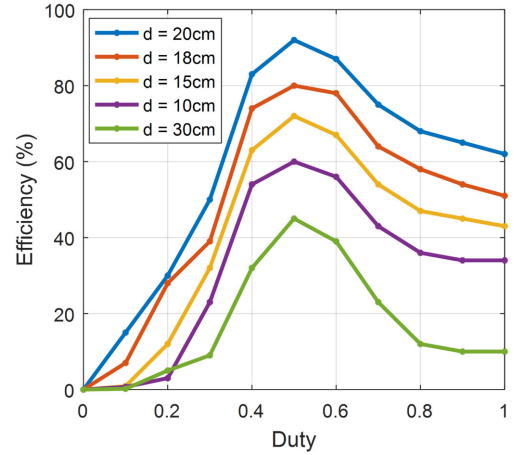

Fig. 24.   Efficiency vs. duty plot for different coupling separation values.

A. Analysis and Discussion of Hardware Outcomes

As proposed in the CSI design section, the transmitter inductance value is tuned by considering the input inductor of the primary-side converter. The major goals of this tuning are to eliminate reverse current flow, improve wireless power transfer efficiency, and to achieve a higher and flexible coupling separation. The hardware waveforms prove that the reverse current flow is absent from the source side. By considering the efficiency vs. coupling separation plot as shown in Fig. 22, maximum efficiency of 94% is achieved at a coupling separation of 20 cm, which is 20% more than the conventional VSI-based, renewable energy-powered SS-WPT charging efficiency. This makes the proposed system more suitable for renewable energy-powered operations. As mentioned in the previous sections, the low-/medium-powered EVs like e-cycles and e-scooters lack physical stability due to the two-wheeler structure. This criterion points to the misalignment changes during the wireless charging operation. As the developed linear closed loop is ensuring a regulated voltage even for high coupling separation, the linear misalignment tolerance is covered. The angular misalignment tolerance is discussed in this section.

Fig. 24 considers the variation of efficiency against the duty for various distances. As explained earlier, maximum efficiency is associated with a coupling separation of 20 cm. Here also, for a duty of 0.5, efficiency is maximum for each considered case of coupling separation, which proves the mathematical analysis. Here voltage and load are maintained as 25 V and 10 Ω, respectively. At each distance cases, maximum efficiency is obtained at a duty of 0.5.

In addition to the improved coupling separation and higher transfer efficiency, another objective of this proposed design is to obtain higher misalignment tolerance, which will incorporate flexibility to the charging mechanism. As the linear misalignment tolerance is already verified in Fig. 22, angular misalignment-tolerance needs to be validated. Initially, the misalignment is analyzed through simulation. Then, the same study is carried out in implemented hardware. Fig. 25 shows the analysis of angular displacement. A misalignment of a maximum of 90° is allowed for angular alignment testing. This analysis also

This article has been accepted for inclusion in a future issue of this journal. Content is final as presented, with the exception of pagination.

JOSEPH *et al.*: SYSTEM ARCHITECTURE, DESIGN, AND OPTIMIZATION OF A FLEXIBLE WIRELESS CHARGER 11
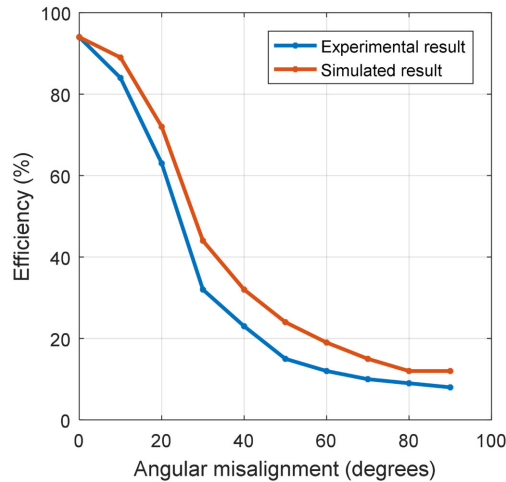
Fig. 25. Efficiency vs. angular misalignment plot.

carried out with respect to the maximum efficiency condition of 20 cm. Up to 10°, the reduction in efficiency is less; then up to 30°, efficiency falls drastically; and beyond 30°, efficiency falls with a reduced slope.

In practical applications of EV charging, misalignment tolerance has huge importance. Here the proposed design is implemented for low-/medium-power EVs like e-bicycles or e-bikes. The major disadvantages of these vehicles are their poor physical stability due to two-tire structure. We cannot expect a perfect parallel posture for e-bicycles. As per the analyzed results, the proposed design provides high efficiency even for worst-case misalignment.

VI. CONCLUSION

Wireless charging of EVs is becoming the era-defining technology in the transportation sector. Several types of WPT techniques were introduced for EV charging, each having its own merits and demerits. The true essence of EV transportation concept will be achieved only with the integration of renewable energy sources in the context of energy conservation. But renewable energy integration along with flexible charging distance and improved transfer efficiency cannot be achieved with the conventional topologies. A prototype for 96-W current-fed SS-WPT is designed for an electric bicycle. The major achievements are listed as follows.

1) A coil tuning mechanism is implemented, which successfully mitigated the reverse current flow in the wireless charger without affecting the performance.
2) A maximum coupling separation of 300 mm is achieved for transferring the rated power.
3) A maximum efficiency of 94% is achieved for a coupling separation of 200 mm, which is better than any known renewable energy-based low-power WPT systems.
4) A high level of linear and horizontal misalignment tolerance is achieved.
5) The proposed linear closed-loop control mechanism successfully regulates the output voltage irrespective of the

variations in coupling separation, input voltage, load, and alignment.

The proposed wireless charging topology is designed for low-/medium-power EV charging applications. Since the performance is promising, it can be extended to charge high-power EVs. By modifying the converter circuit to bidirectional mode, a high efficient vehicle-to-grid system can be implemented as future work.

REFERENCES

[1] C. C. Chan, A. Bouscayrol, and K. Chen, "Electric, hybrid, and fuel-cell vehicles: Architectures and modeling," *IEEE Trans. Veh. Technol.*, vol. 59, no. 2, pp. 589–598, Feb. 2010.

[2] N. Shafiei, M. Ordonez, M. A. S. Tokaldani, and S. A. Arefifar, "PV battery charger using an $L3C$ resonant converter for electric vehicle applications," *IEEE Trans. Transp. Electrific.*, vol. 4, no. 1, pp. 108–121, Mar. 2018.

[3] R. Matulka, *Timeline: History of the Electric Car*. U.S Department of Energy, 2014, pp. 1–5.

[4] C. C. Chan and K. T. Chau, *Modern Electric Vehicle Technology*. New York, NY, USA: Oxford University Press, 2001, pp. 5–7.

[5] M. Yilmaz and P. T. Krein, "Review of battery charger topologies, charging power levels, and infrastructure for plug-in electric and hybrid vehicles," *IEEE Trans. Power Electron.*, vol. 28, no. 5, pp. 2151–2169, May 2013.

[6] A. N. Azad, A. Echols, V. A. Kulyukin, R. Zane, and Z. Pantic, "Analysis, optimization, and demonstration of a vehicular detection system intended for dynamic wireless charging applications," *IEEE Trans. Transp. Electrific.*, vol. 5, no. 1, pp. 147–161, Mar. 2019.

[7] S. Niu, H. Xu, Z. Sun, Z. Y. Shao, and L. Jian, "The state-of-the-arts of wireless electric vehicle charging via magnetic resonance: Principles, standards and core technologies," *Renewable Sustain. Energy Rev.*, vol. 114, 2019. Art. no. 109302.

[8] D. Zhang, H. Lin, Q. Zhang, S. Kang, and Z. Lu, "Analysis, design, and implementation of a single-stage multipulse flexible-topology thyristor rectifier for battery charging in electric vehicles," *IEEE Trans. Energy Convers.*, vol. 34, no. 1, pp. 47–57, Mar. 2019.

[9] R. Collin, Y. Miao, A. Yokochi, P. Enjeti, and A. von Jouanne, "Advanced electric vehicle fast-charging technologies," *Energies*, vol. 12, no. 10, p. 1839, 2019.

[10] R. R. Deshmukh and M. S. Ballal, "An energy management scheme for grid connected EVs charging stations," in *Proc. Int. Conf. Power Instrum. Control Comput.*, 2018, pp. 1–6.

[11] V. Monteiro, J. C. Ferreira, A. A. N. Melendez, C. Couto, and J. L. Afonso, "Experimental validation of a novel architecture based on a dual-stage converter for off-board fast battery chargers of electric vehicles," *IEEE Trans. Veh. Technol.*, vol. 67, no. 2, pp. 1000–1011, Feb. 2018.

[12] J. Reimers, L. Dorn-Gomba, C. Mak, and A. Emadi, "Automotive traction inverters: Current status and future trends," *IEEE Trans. Veh. Technol.*, vol. 68, no. 4, pp. 3337–3350, Apr. 2019.

[13] F. Ahmad, M. S. Alam, S. M. Shariff, and M. Krishnamurthy, "A cost-efficient approach to EV charging station integrated community microgrid: A case study of Indian power market," *IEEE Trans. Transp. Electrific.*, vol. 5, no. 1, pp. 200–214, Mar. 2019.

[14] P. K. Joseph and D. Elangovan, "A review on renewable energy powered wireless power transmission techniques for light electric vehicle charging applications," *Elsevier J. Energy Storage*, vol. 16, pp. 145–155, 2018.

[15] Y. J. Jang, E. S. Suh, and J. W. Kim, "System architecture and mathematical models of electric transit bus system utilizing wireless power transfer technology," *IEEE Syst. J.*, vol. 10, no. 2, pp. 495–506, Jun. 2016.

[16] A. Kurs, A. Karalis, R. Moffatt, J. D. Joannopoulos, P. Fisher, and M. Soljacic, "Wireless power transfer via strongly coupled magnetic resonances," *Science*, vol. 5, pp. 83–86, 2007.

[17] S. Byeong-Mun, R. Kratz, and S. Gurol, "Contactless inductive power pickup system for Maglev applications," in *Proc. Industry Appl. Conf.*, 2002, pp. 1586–1591.

[18] J. T. Boys, G. A. Covic, and A. W. Green, "Stability and control of inductively coupled power transfer systems," *IEEE Proc. Electric Power Appl.*, vol. 147, no. 1, pp. 37–43, Jan. 2000.

[19] C.-S. Wang, G. A. Covic, and O. H. Stielau, "Power transfer capability and bifurcation phenomena of loosely coupled inductive power transfer systems," *IEEE Trans. Ind. Electron.*, vol. 51, no. 1, pp. 148–157, Feb. 2004.

[20] W. Jiang, S. Xu, N. Li, Z. Lin, and B. W. Williams, "Wireless power charger for light electric vehicles," in *Proc. IEEE 11th Int. Conf. Power Electron. Drive Syst.*, 2015, pp. 562–566.

[21] W. Li, H. Zhao, J. Deng, S. Li, and C. C. Mi, "Comparison study on SS and double-sided LCC compensation topologies for EV/PHEV wireless chargers," *IEEE Trans. Veh. Technol.*, vol. 65, no. 6, pp. 4429–4439, Jun. 2016.

[22] Y. Yao, Y. Wang, J. M. A. Álvarez, X. Liu, H. Cheng, and D. Xu, "Efficiency-based design optimisation of a double-sided LCL compensated wireless power transfer system," *IET Power Electron.*, vol. 12, no. 10, pp. 2436–2446, 2019.

[23] C. Jiang, K. T. Chau, W. Liu, C. Liu, W. Han, and W. H. Lam, "An LCC compensated multiple-frequency wireless motor system," *IEEE Trans. Ind. Inform.*, vol. 15, no. 11, pp. 6023–6034, Nov. 2019.

[24] J. I. Itoh, K. Noguchi, and K. Orikawa, "System design of electric assisted bicycle using EDLCs and wireless charger," in *Proc. IEEE Int. Power Electron. Conf.*, 2014, pp. 2277–2284.

[25] F. Pellitteri, G. Ala, M. Caruso, S. Ganci, and R. Miceli, "Physiological compatibility of wireless chargers for electric bicycles," in *Proc. IEEE Int. Conf. Renewable Energy Res. Appl.*, 2015, pp. 1354–1359.

[26] S. Li, W. Li, J. Deng, T. D. Nguyen, and C. C. Mi, "A double-sided LCC compensation network and its tuning method for wireless power transfer," *IEEE Trans. Veh. Technol.*, vol. 64, no. 6, pp. 2261–2273, Jun. 2015.

[27] S. Samanta and A. K. Rathore, "Wireless power transfer technology using full-bridge current-fed topology for medium power applications," *Power Electron. IET*, vol. 9, no. 9, pp. 1903–1913, 2016.

[28] Delft University of Technology, "First solar-powered wireless charging station for electric bikes," *PHYS.ORG*, 2016, pp. 20–24.

[29] J. Hirai, T.-W. Kim, and A. Kawamura, "Study on intelligent battery charging using inductive transmission of power and information," *IEEE Trans. Power Electron.*, vol. 15, no. 2, pp. 335–345, Mar. 2000.

[30] N. H. Kutkut and K. W. Klontz, "Design considerations for power converters supplying the SAE J-1773 electric vehicle inductive coupler," in *Proc. Appl. Power Electron. Conf. Expo.*, 1997, pp. 841–847.

[31] Y. Zhang, T. Kan, Z. Yan, Y. Mao, Z. Wu, and C. C. Mi, "Modeling and analysis of series-none compensation for wireless power transfer systems with a strong coupling," *IEEE Trans. Power Electron.*, vol. 34, no. 2, pp. 1209–1215, Feb. 2019.

[32] Z. Li, K. Song, G. Wei, J. Jiang, and C. Zhu, "A 3 kW wireless power transfer system for sightseeing car supercapacitor charge," *IEEE Trans. Power Electron.*, vol. 32, no. 5, pp. 3301–3316, May 2017.

[33] A. P. Hu, J. T. Boys, and G. A. Covic, "ZVS frequency analysis of a current-fed resonant converter," in *Proc. 7th IEEE Int. Power Electron. Congr.*, 2000, pp. 217–221.

[34] P. K. Joseph, D. Elangovan, and G. Arunkumar, "Linear control of wireless charging for electric bicycles," *Appl. Energy*, vol. 255, 2019, Art. no. 113898.

[35] M. Chigira, Y. Nagatsuka, Y. Kaneko, S. Abe, T. Yasuda, and A. Suzuki, "Small-size light-weight transformer with new core structure for contactless electric vehicle power transfer system," in *Proc. IEEE Energy Convers. Congr. Expo.*, 2011, pp. 260–266.

Peter K. Joseph was born in Kerala, India, in 1993. He received the B.Tech degree in electrical and electronics engineering from M.G University, Kerala, India, in 2014, and the M.Tech degree in power electronics, with university rank, from Cochin University of Science and Technology, Kerala, India, in 2016. He is currently working toward the Ph.D. degree on renewable energy-powered wireless charging of electric vehicles at the Vellore Institute of Technology (VIT) University, Vellore, India.

Since 2017, he has been working as an Assistant Professor with the School of Electrical Engineering, VIT University. He worked as a Project Trainee with Indian Space Research Organization, on digital control of space grade electronic power conditioners from 2015 to 2016. He worked as an Executive Automation Engineer with Cedar Technologies. His research interests include wireless power transmission, electric vehicles, electronic power conditioners, etc.

Mr. Joseph's works on automation were selected as the Best Technical Project in India multiple times by different national and international agencies, including IEEE in 2015.

Devaraj Elangovan received the B.E. degree in electrical and electronics engineering from Madras University, Tamilnadu, India in 2003. the M.Tech degree in power electronics and drives from Sri Venkateswara college of Engineering (Anna University), Tamilnadu, India, in 2005, and the Ph.D degree in analysis, design and implementation of high gain dc–dc converters for fuel cell applications from the Vellore Institute of Technology, University, Vellore in 2016.

He was a Lecturer in Power Electronics and Converters with the Abdul Hakeem College of Engineering and Technology, India. Later he joined the Sri Venkateswara College of Engineering as an Assistant Professor in the same domain. He was with the Power Electronics and Energy Department of Vellore Institute of Technology, India as Assistant Professor. Now he is an Associate Professor and Head of the same department. With the expertise in electric vehicles and power electronics, he has guided a doctoral research on wireless charging of electric vehicles. He holds three patents and authored or coauthored 63 research papers with cumulative Thomson Reuters (Web of Science) Impact Factor more than 25. Furthermore, his research contribution results in more than 50 citations with an H-index of 4. His research contribution is extended toward the development of high-efficient wireless power transmission system for electric vehicle charging applications. His current research interests include the development of a universal wireless charger for the electric vehicle application using machine learning techniques.

Dr. Elangovan has secured (as a Co-Principal Investigator) an International funded project worth 49,800.00 Euro from The Royal Academy of Engineering, London, which is a collaboration between India and the United Kingdom.

Padmanaban Sanjeevikumar (Senior Member, IEEE) received the bachelor's degree from the University of Madras, Chennai, India, in 2002, the master's degree (Hons.) from Pondicherry University, Puducherry, India, in 2006, and the Ph.D. degree from the University of Bologna, Bologna, Italy, in 2012, all in electrical engineering.

He was an Associate Professor with VIT University from 2012 to 2013. In 2013, he joined the National Institute of Technology, India, as a Faculty Member. In 2014, he was invited as a Visiting Researcher at the Department of Electrical Engineering, Qatar University, Doha, Qatar, funded by the Qatar National Research Foundation (Government of Qatar). He continued his research activities with Dublin Institute of Technology, Dublin, Ireland, in 2014. He was an Associate Professor with the Department of Electrical and Electronics Engineering, University of Johannesburg, Johannesburg, South Africa, from 2016 to 2018. Since 2018, he has been a Faculty Member with the Department of Energy Technology, Aalborg University, Esbjerg, Denmark. He has authored more than 300 scientific papers.

Dr. Padmanaban was the recipient of the Best Paper cum Most Excellence Research Paper Award from International Conference on Sustainable Energy and Intelligent Systems'13, IET International Conference on Clean Energy and Technology'16, IEEE- Electrical Engineering, Computer Science and Informatics'19, and IEEE-Conference on Energy Conversion'19, and five best paper awards from International Conference on Emerging Trends and Advances in Electrical Engineering and Renewable Energy'16 sponsored Lecture Notes in Electrical Engineering, Springer book. He is a Fellow of the Institution of Engineers, India, the Institution of Electronics and Telecommunication Engineers, India, and the Institution of Engineering and Technology, U.K. He is an Editor/Associate Editor/Editorial Board Member for refereed journals, in particular the IEEE SYSTEMS JOURNAL, IEEE TRANSACTIONS ON INDUSTRY APPLICATIONS, IEEE ACCESS, *IET Power Electronics*, and *International Transaction on Electrical Energy Systems*, *Wiley*, and the Subject Editor for the *IET Renewable Power Generation*, *IET Generation, Transmission and Distribution, and FACTS journal* (Canada).